Magnitude- and orientation-steerable beam deflection in self-induced harmonic potentials

Juan Chen,* Guiqin Cai,* Daquan Lu,† and Wei Hu‡
Guangdong Provincial Key Laboratory of Nanophotonic Functional Materials and Devices, South China Normal University, Guangzhou 510631, China

(Received 20 March 2019; revised manuscript received 31 July 2019; published 14 October 2019)

In self-induced harmonic potentials, the coaxial superposition of a fundamental Gaussian beam and a (0,1) mode Laguerre-Gaussian beam yields a two-dimensional (2D)–deflection-steerable breathing beam. The magnitude (orientation) of the deflection can be steered by tuning the ratio (initial phase difference) between the two input constituent beams. Besides, the beam rotates around the deflecting straight trajectory the mass center (not the constituent beams' center) undergoes. The results provide an approach for the 2D steering of beam trajectory, which might be of interest for the applications in all-optical information processing.

DOI: 10.1103/PhysRevA.100.043820

I. INTRODUCTION

In recent years, the propagation of light beams in media with harmonic potentials has aroused considerable interest. Harmonic potentials act as effective tools to manipulate the evolution of beams and give rise to various interesting effects, such as the periodic focusing [1], the designable self-Fourier beams [2], the shape-invariant rotating beams [3], the anharmonic oscillation [4–6], the phase transition [5,6], and the periodic inversion [6,7]. We can roughly classify harmonic potentials into two categories: the medium-induced harmonic potentials and the self-induced harmonic potentials. The medium-induced harmonic potentials can be easily achieved in linear gradient-index media, whereas the self-induced harmonic potentials are closely related to the nonlocal nonlinear propagation of beams. It has been found that, in the case of strongly nonlocal nonlinearity, the nonlinearity-induced change of refractive index acts as a harmonic potential, and therefore the nonlinear Schrödinger equation can be simplified to a linear model called the Snyder-Mitchell model (SMM) [8]. Based on the SMM, various localized shape-invariant waves, such as vortex solitons [9–12], multipole solitons [13–15], and soliton clusters [16], have been predicted. Some interesting effects related to the strongly nonlocal nonlinearity, such as large phase shift [17], power-variation-induced three-dimensional nonuniform scaling [18], and self-induced fractional Fourier transform [19], have been revealed on the basis of the SMM.

In this paper, we introduce another effect in self-induced harmonic potentials: magnitude- and orientation-steerable beam deflection. The input field of the deflecting beam is a combined field composed of a fundamental Gaussian beam and a (0,1) mode Laguerre-Gaussian beam. The beam experiences deflection and rotation during propagation. It is particularly interesting that the magnitude and orientation of the deflection can be steered by tuning the ratio and the initial phase difference between the two input constituent beams, respectively.

II. THE ANALYTICAL SOLUTION

Let us first recall the governing equation. We consider a beam propagating in a self-induced harmonic potential, in which the evolution of the complex amplitude envelope of the field [represented as $\Psi(x, y, z)$] is governed by the Schrödinger equation

$$2ik\frac{\partial\Psi}{\partial z}+\frac{\partial^2\Psi}{\partial x^2}+\frac{\partial^2\Psi}{\partial y^2}-V(\mathbf{r},z)\Psi=0, \tag{1}$$

where k is the wave number in the media without nonlinearity. $V(\mathbf{r}, z)$ is the self-induced harmonic potential. It has been discovered that when a beam is propagating in the strongly nonlocal nonlinear media, the beam itself would induce a power-dependent harmonic potential [8],

$$V(\mathbf{r},z)=k^2\gamma^2P_0|\mathbf{r}-\mathbf{r}_c(z)|^2, \tag{2}$$

where γ is a coefficient related to the nonlocal degree of the nonlinearity. $\mathbf{r}=(x, y)$, $\mathbf{r_c}=(x_c, y_c)$ is the mass center of the beam. $P_0=\int_{-\infty}^{\infty}|\Psi(\mathbf{r},0)|^2dxdy$ is the power of the input field.

For most beams, the transverse location of the mass center stays invariant during propagation [i.e., $\mathbf{r}_c(z)\equiv 0$]; therefore, Eq. (1) is deduced to

$$2ik\frac{\partial\Psi}{\partial z}+\frac{\partial^2\Psi}{\partial x^2}+\frac{\partial^2\Psi}{\partial y^2}-k^2\gamma^2P_0r^2\Psi=0, \tag{3}$$

which is the so-called SMM. [We call it the *standard* SMM here. Correspondingly, we call Eq. (1) the *modified* SMM.]

However, in this paper we construct a special type of beam, of which the potential transversely moves with the mass center of the beam. This type of beam is a combined field resulting from the coaxial superposition of a fundamental Gaussian beam and a (0,1) mode Laguerre-Gaussian beam,

$$\Psi(\mathbf{r},0)=\Psi_1(\mathbf{r},0)+\Psi_2(\mathbf{r},0), \tag{4}$$

*Both authors contributed equally to this work.
†ludq@scnu.edu.cn
‡huwei@scnu.edu.cn

where

$$\Psi_1(\mathbf{r},0)=\Psi_0\exp\left(-\frac{r^2}{2w_0^2}\right), \tag{5}$$

$$\begin{aligned}\Psi_2(\mathbf{r},0)&=b\Psi_0\frac{r}{w_0}\exp\left(-\frac{r^2}{2w_0^2}\right)\exp\left[i\varphi(0)\right]\exp\left(i\delta\right)\\&=b\Psi_0\frac{x+iy}{w_0}\exp\left(-\frac{r^2}{2w_0^2}\right)\exp\left(i\delta\right),\end{aligned} \tag{6}$$

Ψ_0 is the amplitude coefficient which ensures that $P_0=\int_{-\infty}^{\infty}|\Psi(\mathbf{r},0)|^2dxdy$, b is the ratio coefficient of the two constituent beams, δ is the initial phase difference between the two constituent beams, w_0 is the width of the beam waist, and $\varphi(\cdot)$ is the azimuthal angle around the beam center of the constituent beams.

Because of the mathematical complexity, it is not easy to directly solve the *modified* SMM [i.e., Eq. (1)] for the input field shown in Eq. (4). However, the *modified* SMM can be transformed to an equation which is in form the same as the *standard* SMM, by utilizing the technique of variable transformation [20], as follows. According to Ehrenfest's theorem, the mass center of the field undergoes a straight trajectory, i.e.,

$$\mathbf{r}_c(z)=\mathbf{r}_c(0)+\frac{\mathbf{M}}{P_0}z, \tag{7}$$

where

$$\mathbf{r}_c(0)=\int_{-\infty}^{\infty}\mathbf{r}|\Psi(\mathbf{r},0)|^2dxdy/P_0 \tag{8}$$

is the position of the mass center at the entrance plane and

$$\mathbf{M}=\frac{i}{2k}\int_{-\infty}^{\infty}(\Psi\nabla_\perp\Psi^*-\Psi^*\nabla_\perp\Psi)dxdy \tag{9}$$

is the transverse momentum of the input field. Therefore, if one introduces a comoving reference frame

$$\mathbf{r}'(z)=\mathbf{r}-\mathbf{r}_c(z),\ z'=z, \tag{10}$$

and makes the variable transformation

$$\Psi(\mathbf{r},z)=\Phi(\mathbf{r}',z')\exp\left(\frac{ik\mathbf{M}\cdot\mathbf{r}'}{P_0}+\frac{ikM^2}{2P_0^2}z'\right), \tag{11}$$

Eq. (1) becomes [20]

$$2ik\frac{\partial\Phi}{\partial z'}+\frac{\partial^2\Phi}{\partial x'^2}+\frac{\partial^2\Phi}{\partial y'^2}-k^2\gamma^2P_0r'^2\Phi=0, \tag{12}$$

which is in form the same as the *standard* SMM [i.e., Eq. (3)] and is mathematically simpler than the *modified* SMM [i.e., Eq. (1)]. In the following, we still call Eq. (12) the *standard* SMM.

For the *standard* SMM [i.e., Eq. (12)] in the comoving reference frame $(\mathbf{r}',z')$, the input field becomes

$$\Phi(\mathbf{r}',0)=\Phi_1(\mathbf{r}',0)+\Phi_2(\mathbf{r}',0), \tag{13}$$

where

$$\Phi_1(\mathbf{r}',0)=\Psi_0\exp\left[-\frac{|\mathbf{r}'+\mathbf{r}_c(0)|^2}{2w_0^2}\right]\exp\left(-\frac{ik\mathbf{M}\cdot\mathbf{r}'}{P_0}\right), \tag{14}$$

$$\Phi_2(\mathbf{r}',0)=b\Phi_1(\mathbf{r}',0)\frac{[x'+x_c(0)]+i[y'+y_c(0)]}{w_0}\exp(i\delta). \tag{15}$$

Comparing Eqs. (12) and (13) with Eqs. (1) and (2) in our previous work (i.e., Ref. [3]), we found that the input beam in the comoving reference frame $(\mathbf{r}',z')$ in the self-induced harmonic potential is analogous to the input beam with the initial kick $-k\mathbf{M}/P_0$ and the initial transverse displacement $-\mathbf{r}_c(0)$ in the laboratory reference frame in the medium-induced harmonic potential. Therefore, following the method used in Ref. [3], we can straightforwardly get the analytical solution of Eq. (12),

$$\Phi(\mathbf{r}',z')=[\Phi_1(\mathbf{r}',z')+\Phi_2(\mathbf{r}',z')]\exp[i\mathbf{u}(z')\cdot\mathbf{r}'+i\zeta(z')], \tag{16}$$

where

$$\Phi_1(\mathbf{r}',z')=\Psi_0\frac{w_0}{w(z')}\exp\left[-\frac{|\mathbf{r}'+\mathbf{s}(z')|^2}{2w^2(z')}\right]\exp\left[\frac{ik|\mathbf{r}'+\mathbf{s}(z')|^2}{2R(z')}\right]\exp\left(-i\left\{a\pi+\arctan\left[\frac{z_{p0}}{z_0}\tan\left(\frac{z'}{z_{p0}}\right)\right]\right\}\right), \tag{17}$$

$$\Phi_2(\mathbf{r}',z')=b\Phi_1(\mathbf{r}',z')\frac{|\mathbf{r}'+\mathbf{s}(z')|}{w(z')}\exp[i\varphi(z')]\exp(i\delta)\exp\left(-i\left\{a\pi+\arctan\left[\frac{z_{p0}}{z_0}\tan\left(\frac{z'}{z_{p0}}\right)\right]\right\}\right), \tag{18}$$

$$w(z')=\frac{w_0\left\{1+\left[\frac{z_{p0}}{z_0}\tan\left(\frac{z'}{z_{p0}}\right)\right]^2\right\}^{1/2}}{\left[1+\tan^2\left(\frac{z'}{z_{p0}}\right)\right]^{1/2}}, \tag{19}$$

$$R(z')=\frac{1}{1+\tan^2\left(\frac{z'}{z_{p0}}\right)}\frac{z_{p0}\tan\left(\frac{z'}{z_{p0}}\right)}{\frac{1}{1+1/\left[\frac{z_{p0}}{z_0}\tan\left(\frac{z'}{z_{p0}}\right)\right]^2}-\frac{1}{\left[1+1/\tan^2\left(\frac{z'}{z_{p0}}\right)\right]}}, \tag{20}$$

$$\mathbf{s}(z')=\frac{1}{(-1)^a\left[1+\tan^2\left(\frac{z'}{z_{p0}}\right)\right]^{1/2}}\left[\mathbf{r}_c(0)+\frac{\mathbf{M}}{P_0}z_{p0}\tan\left(\frac{z'}{z_{p0}}\right)\right], \tag{21}$$

$$\mathbf{u}(z')=\frac{1}{(-1)^a\left[1+\tan^2\left(\frac{z'}{z_{p0}}\right)\right]^{1/2}}\left[k\frac{\mathbf{r}_c(0)}{z_{p0}}\tan\left(\frac{z'}{z_{p0}}\right)-k\frac{\mathbf{M}}{P_0}\right], \tag{22}$$

$$\zeta(z')=\frac{k}{4}\left[\frac{r_c^2(0)}{z_{p0}}-\frac{M^2z_{p0}}{P_0^2}\right]\sin\left(\frac{2z'}{z_{p0}}\right)+k\frac{\mathbf{M}\cdot\mathbf{r}_c(0)}{P_0}\sin^2\left(\frac{z'}{z_{p0}}\right), \tag{23}$$

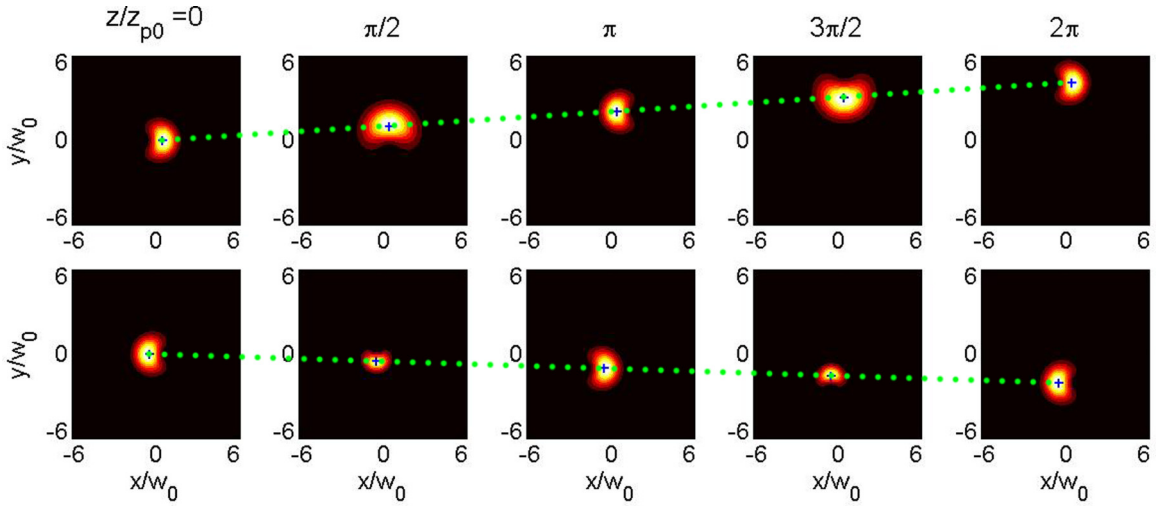

FIG. 1. Propagation dynamics of the deflecting breathing beam for different input powers P_0 and different initial phase differences δ between the two input constituent beams. Upper row: $P_0 = 0.5(z_0\gamma)^{-2}$, $\delta = 0$. Bottom row: $P_0 = 2(z_0\gamma)^{-2}$, $\delta = \pi$. The ratio coefficient $b = 1$.

$a(z') = 1/\pi\{z'/z_{p0} - \arctan[\tan(z'/z_{p0})]\}$, $z_{p_0} = (\gamma^2 P_0)^{-1/2}$, and $z_0 = kw_0^2$.

Therefore, from Eqs. (10), (11), and (16), we can obtain the analytical solution of the *modified* SMM [i.e., Eq. (1)] in the laboratory reference frame,

$$\Psi(\mathbf{r}, z) = [\Psi_1(\mathbf{r}, z) + \Psi_2(\mathbf{r}, z)]\exp[i\mathbf{v}(z)\cdot\mathbf{r} + i\alpha(z)], \quad (24)$$

where

$$\Psi_1(\mathbf{r}, z) = \Psi_0 \frac{w_0}{w(z)} \exp\left[-\frac{|\mathbf{r} - \mathbf{r}_0(z)|^2}{2w^2(z)}\right] \exp\left[\frac{ik|\mathbf{r} - \mathbf{r}_0(z)|^2}{2R(z)}\right] \times \exp\left(-i\left\{a\pi + \arctan\left[\frac{z_{p0}}{z_0}\tan\left(\frac{z}{z_{p0}}\right)\right]\right\}\right), \quad (25)$$

$$\Psi_2(\mathbf{r}, z) = b\Psi_1(\mathbf{r}, z)\frac{|\mathbf{r} - \mathbf{r}_0(z)|}{w(z)} \exp[i\varphi(z)]\exp(i\delta) \times \exp\left(-i\left\{a\pi + \arctan\left[\frac{z_{p0}}{z_0}\tan\left(\frac{z}{z_{p0}}\right)\right]\right\}\right), \quad (26)$$

$$\alpha(z) = \zeta(z) - \mathbf{r}_c(z)\cdot\left[k\frac{\mathbf{r}_c(0)}{z_{p0}}\sin\left(\frac{z}{z_{p0}}\right) - k\frac{\mathbf{M}}{P_0}\cos\left(\frac{z}{z_{p0}}\right) + k\frac{\mathbf{M}}{P_0}\right] + \frac{kM^2}{2P_0^2}z, \quad (27)$$

$$\mathbf{r}_0(z) = \mathbf{r}_c(z) - \mathbf{s}(z), \quad (28)$$

$$\mathbf{v}(z) = k\frac{\mathbf{M}}{P_0} + \mathbf{u}(z). \quad (29)$$

Equation (24) is the main result of the 2D-deflection-steerable breathing beam in the self-induced harmonic potential. The propagation properties will be discussed in detail below.

III. PROPAGATION PROPERTIES

We discuss the propagation properties of the deflecting breathing beam based on Eq. (24). As shown in Fig. 1, during propagation, the beam pattern stays shape invariant, but the beam size increases and decreases alternatively (that is why we call it a breathing beam). It is particularly interesting is that (i) the mass center of the beam undergoes a steerable straight trajectory deflecting from the z axis and (ii) the pattern rotates around the trajectory the mass center (not the constituent beams' center) undergoes.

A. Magnitude- and orientation-steerable deflection

According to Eq. (7), it is the transverse momentum that induces the deflection of the beam. For the input field shown in Eq. (4), the slope of the trajectory of the mass center with respect to the z axis is

$$\mathbf{M}_p = \frac{\mathbf{M}}{P_0} = \frac{b\sin\delta}{kw_0(1+b^2)}\mathbf{e}_x + \frac{b\cos\delta}{kw_0(1+b^2)}\mathbf{e}_y. \quad (30)$$

Obviously, the magnitude of the slope is

$$|\mathbf{M}_p| = \frac{b}{kw_0(1+b^2)}. \quad (31)$$

As shown in Fig. 2, with the increase of the ratio parameter b, the deflection slope $|\mathbf{M}_p|$ increases first, then arrives its maximum at $b = 1$, and then decreases with b. As expected, there is no deflection (i.e., $|\mathbf{M}_p| = 0$) when $b = 0$ or ∞, which means that only one constituent beam is input. Besides, the azimuth orientation of the deflection is determined by the initial phase difference (i.e., δ) between the two constituent beams through the relation

$$\theta_M = \frac{\pi}{2} - \delta. \quad (32)$$

Therefore, according to Eqs. (31) and (32), the amplitude (i.e., $|\mathbf{M}_p|$) and orientation (i.e., θ_M) of the deflection can be steered by tuning the ratio coefficient b and the initial phase difference δ, respectively.

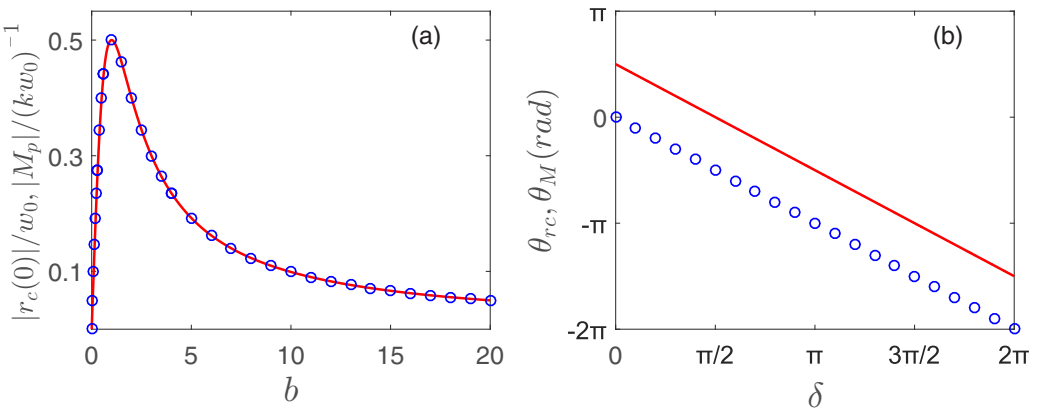

FIG. 2. (a) The magnitude for the slope of the trajectory ($|M_p|$, solid line) and for the initial displacement of the mass center from the center of the constituent beams [$r_c(0)$, circle symbols] vs the ratio coefficient b of the two input constituent beams. (b) The azimuth orientation for the deflection (θ_M, solid line) and for the initial displacement of the mass center from the center of the constituent beams (θ_{rc}, circle symbols) vs the initial phase difference δ between the two input constituent beams.

The deflection is closely related to the initial displacement of the mass center for the combined field from the center of the constituent beams. Based on Eq. (8), we have

$$\mathbf{r}_c(0) = \frac{bw_0 \cos\delta}{1+b^2}\mathbf{e}_x - \frac{bw_0 \sin\delta}{1+b^2}\mathbf{e}_y, \tag{33}$$

of which the amplitude and the azimuth orientation are

$$|\mathbf{r}_c(0)| = \frac{bw_0}{1+b^2} \tag{34}$$

and

$$\theta_{r_c} = -\delta, \tag{35}$$

respectively. Comparing Eq. (31) with Eq. (34), we have an interesting relation between the trajectory slope $\mathbf{M}_p$ and the initial displacement $\mathbf{r}_c(0)$, reads

$$\frac{|\mathbf{r}_c(0)|}{|\mathbf{M}_p|} = kw_0^2 = z_0. \tag{36}$$

In addition, according to Eqs. (32) and (35), we have $\theta_{r_c} = \theta_M - \pi/2$, which means that the beam always deflects in the direction which is vertical to the orientation of the initial displacement of the mass center, as shown in Figs. 1 and 2(b).

B. Rotation of the beam around the deflecting trajectory

Beyond the deflection of the trajectory of the mass center, the beam also elliptically rotates around the deflecting trajectory during propagation. In fact, the rotation results from three aspects: the breath, the rotation of the combined field around the constituent beams' center, and the rotation of constituent beams' center around the mass center. The synchronous evolution of the three aspects results in the elliptical rotation of the intensity pattern around the trajectory of the mass center.

First, we study the evolution of the displacement of the constituent beams' center [i.e., $\mathbf{r}_0(z)$] from the mass center [i.e., $\mathbf{r}_c(z)$] of the combined field. According to Eq. (28), the displacements in the x and y directions are

$$x_0(z) - x_c(z) = -\left[\frac{M_x^2}{P_0^2}z_{p0}^2 + r_{cx}^2(0)\right]^{1/2} \cos\left[\left(\frac{z}{z_{p0}}\right) + \theta_x\right] \tag{37}$$

and

$$y_0(z) - y_c(z) = -\left[\frac{M_y^2}{P_0^2}z_{p0}^2 + r_{cy}^2(0)\right]^{1/2} \cos\left[\left(\frac{z}{z_{p0}}\right) + \theta_y\right], \tag{38}$$

respectively, where

$$\theta_x = \arctan\left[\frac{-M_x z_{p0}}{P_0 r_{cx}(0)}\right] + \chi[r_{cx}(0)],$$
$$\theta_y = \arctan\left[\frac{-M_y z_{p0}}{P_0 r_{cy}(0)}\right] + \chi[r_{cy}(0)],$$

$\chi(\xi) = 0$ (for $\xi \geqslant 0$) or π (for $\xi < 0$). The oscillations in the x and y directions would result in the elliptical rotation of the constituent beams' center [i.e., $\mathbf{r}_0(z)$] around the mass center [i.e., $\mathbf{r}_c(z)$] of the combined field with the period $2\pi z_{p0}$, just as the beam does in the medium-induced harmonic potential [3].

Second, we study the evolution of the displacement of an arbitrary individual point A [located at $\mathbf{r}_A(z)$] in the intensity pattern from the constituent beams' center [i.e., $\mathbf{r}_0(z)$]. It might be constructive to explain the reason for the rotation of the intensity pattern in advance. According to Eq. (24), the intensity of the combined field is

$$|\Psi(\mathbf{r}, z)|^2 = \Psi_0^2 \frac{w_0^2}{w^2(z)} \exp\left[-\frac{|\mathbf{r}-\mathbf{r}_0(z)|^2}{w^2(z)}\right] \left|1 + b\frac{|\mathbf{r}-\mathbf{r}_0(z)|}{w(z)} \times \exp\left[i\varphi(z) - i\varphi_0(z)\right]\right|^2, \tag{39}$$

where

$$\varphi_0(z) = -\delta + \delta_g(z), \tag{40}$$

$$\delta_g(z) = a\pi + \arctan\left[\frac{z_{p0}}{z_0}\tan\left(\frac{z}{z_{p0}}\right)\right] \tag{41}$$

is the Gouy phase shift difference between the two constituent beams. At the entrance plane (i.e., $z = 0$), as shown in Eq. (39), it is the phase vortex $\varphi(0)$ that induces the circular asymmetry of the pattern. For example, at the azimuthal angle $\varphi = 0$ ($\varphi = \pi$), the two constituent beams interfere constructively (destructively), and the intensity of the combined field here is stronger (weaker). During propagation, the Gouy phase shift difference $\delta_g(z)$ and thereby $\varphi_0(z)$ increase monotonously; thus, the intensity pattern rotates anticlockwise continuously. At $z = z$, the pattern is rotated by the angle $\delta_g(z)$.

On the other hand, due to the breath of the beam, the evolution of the displacement for the individual point A from the constituent beams' center [i.e., $\mathbf{r}_0(z)$] obeys the relation

$$|\mathbf{r}_A(z) - \mathbf{r}_0(z)| = \frac{w(z)}{w_0}|\mathbf{r}_A(0) - \mathbf{r}_0(0)|. \tag{42}$$

Therefore, in the x and y directions, we have

$$x_A(z) - x_0(z) = |\mathbf{r}_A(z) - \mathbf{r}_0(z)|\cos[\theta_A + \varphi_0(z)] = \left\{\left[\frac{r_{A0}z_{p0}\sin(\theta_A - \delta)}{z_0}\right]^2 + [r_{A0}\cos(\theta_A - \delta)]^2\right\}^{1/2}\cos\left[\left(\frac{z}{z_{p0}}\right) + \gamma_1\right], \tag{43}$$

$$y_A(z) - y_0(z) = |\mathbf{r}_A(z) - \mathbf{r}_0(z)|\sin[\theta_A + \varphi_0(z)] = \left\{\left[\frac{r_{A0}z_{p0}\cos(\theta_A - \delta)}{z_0}\right]^2 + [r_{A0}\sin(\theta_A - \delta)]^2\right\}^{1/2}\cos\left[\left(\frac{z}{z_{p0}}\right) + \gamma_2\right], \tag{44}$$

where

$$r_{A0} = |\mathbf{r}_A(0) - \mathbf{r}_0(0)|,$$

$$\gamma_1 = \arctan\left[\frac{z_{p0}\sin(\theta_A - \delta)}{z_0\cos(\theta_A - \delta)}\right] + \chi[\cos(\theta_A - \delta)],$$

$$\gamma_2 = \arctan\left[\frac{-z_{p0}\cos(\theta_A - \delta)}{z_0\sin(\theta_A - \delta)}\right] + \chi[\sin(\theta_A - \delta)],$$

and θ_A is the angle between the initial azimuthal orientation of the individual point A and that of the mass center [i.e., $\mathbf{r}_c(0)$].

Consequently, according to Eqs. (37), (38), (43), and (44), the motion of the individual point A relative to the mass center $\mathbf{r}_c(z)$ becomes

$$x_A(z) = x_c(z) + \left\{\left[\frac{r_{A0}z_{p0}\sin(\theta_A - \delta)}{z_0} + \frac{M_x}{P_0}z_{p0}\right]^2 + [r_{A0}\cos(\theta_A - \delta) - r_{cx}(0)]^2\right\}^{1/2}\cos\left[\left(\frac{z}{z_{p0}}\right) + \beta_1\right], \tag{45}$$

$$y_A(z) = y_c(z) + \left\{\left[\frac{r_{A0}z_{p0}\cos(\theta_A - \delta)}{z_0} - \frac{M_y}{P_0}z_{p0}\right]^2 + [r_{A0}\sin(\theta_A - \delta) - r_{cy}(0)]^2\right\}^{1/2}\cos\left[\left(\frac{z}{z_{p0}}\right) + \beta_2\right], \tag{46}$$

where

$$\beta_1 = \arctan\left[\frac{\frac{r_{A0}z_{p0}\sin(\theta_A - \delta)}{z_0} + \frac{M_x}{P_0}z_{p0}}{r_{A0}\cos(\theta_A - \delta) - r_{cx}(0)}\right] + \chi[r_{A0}\cos(\theta_A - \delta) - r_{cx}(0)],$$

$$\beta_2 = \arctan\left[\frac{-\frac{r_{A0}z_{p0}\cos(\theta_A - \delta)}{z_0} + \frac{M_y}{P_0}z_{p0}}{r_{A0}\sin(\theta_A - \delta) - r_{cy}(0)}\right] + \chi[r_{A0}\sin(\theta_A - \delta) - r_{cy}(0)].$$

Equations (45) and (46) mean that each individual point in the pattern of the combined field rotates elliptically around the deflecting straight trajectory of the mass center (as shown in Fig. 3). When $P_0 > P_c$ ($P_0 < P_c$), the initial position of the individual point is at the endpoint of the major (minor) axis of the ellipse, and the ellipse becomes a circle when $P_0 = P_c$.

IV. DISCUSSION: THE EXTENSION TO THE GENERAL CASE OF NONLOCAL NONLINEARITY

The analytical results in Secs. II and III are based on the assumption that the combined beam is propagating in a self-induced harmonic potential, which is corresponding to the limit case of strongly nonlocal nonlinearity. Therefore, the question arises of what would happen if the strongly nonlocal nonlinear condition is not satisfied. To answer this question, we extend the study to the general case of nonlocal nonlinearity, in which the potential becomes [21]

$$V(\mathbf{r}, z) = -\frac{2k^2}{n_0}\triangle n, \tag{47}$$

where

$$\triangle n = n_2\int_{-\infty}^{\infty} R(|\mathbf{r} - \mathbf{r}_a|)|\Psi(\mathbf{r}_a, z)|^2 d^2\mathbf{r}_a \tag{48}$$

represents the nonlinear refractive index, $R(\cdot)$ is the nonlinear spatial response function of the media, n_0 is the linear refractive index, n_2 is the nonlinear index coefficient, and

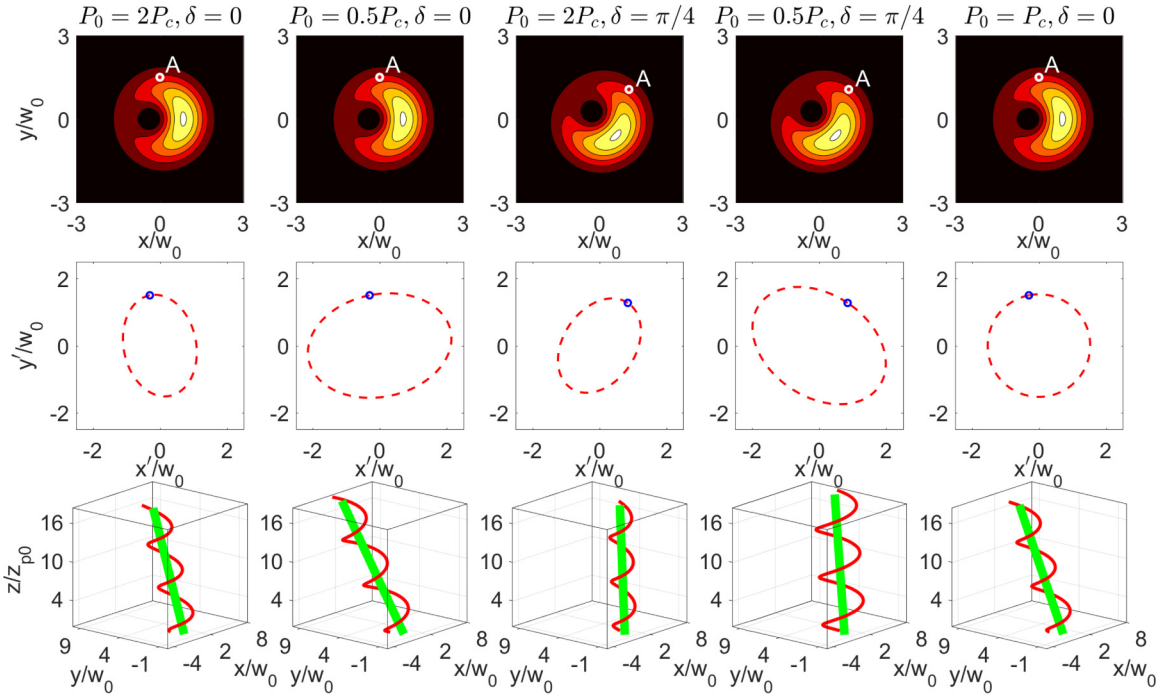

FIG. 3. The trajectory of an individual point in the intensity pattern of the deflecting beam for different input powers and initial phase differences. Upper row: The intensity pattern at the entrance plane. The small circle represents the initial location of the individual point A. Middle row: Projection of the trajectory for the individual point on the x'-y' plane in the comoving reference frame (x', y', z'). Bottom row: The trajectory for the individual point in the 3D space of the laboratory reference frame (x, y, z). The ratio coefficient $b = 3$. $P_c = (z_0\gamma)^{-2}$.

$\mathbf{r_a} = (x_a, y_a)$. In this case, Eq. (1) becomes the general nonlocal nonlinear Schrödinger equation [21]

$$2ik\frac{\partial\Psi}{\partial z} + \frac{\partial^2\Psi}{\partial x^2} + \frac{\partial^2\Psi}{\partial y^2} + \frac{2k^2}{n_0}n_2\Psi\int_{-\infty}^{\infty} R(|\mathbf{r}-\mathbf{r}_a|)|\Psi(\mathbf{r}_a, z)|^2 d^2\mathbf{r}_a = 0. \quad (49)$$

Based on Eq. (49), we first consider the steerable deflection in the case of general nonlocal nonlinearity. As shown in Refs. [20,21], the transverse momentum $\mathbf{M}$ is a conserved quantity for Eq. (49). Therefore, the equation

$$\mathbf{r}_c(z) = \mathbf{r}_c(0) + \frac{\mathbf{M}}{P_0}z = \mathbf{r}_c(0) + \frac{bz\sin\delta}{kw_0(1+b^2)}\mathbf{e}_x + \frac{bz\cos\delta}{kw_0(1+b^2)}\mathbf{e}_y, \quad (50)$$

which describes the deflecting straight trajectory the mass center and thereby the moving potential undergo, is also valid in the general nonlocal case, whatever the degree of nonlocality is. If the ratio parameter $b \neq 0, \infty$, the transverse momentum would be nonzero, and thereby the mass center of the combined field would undergo a 2D steerable deflecting straight trajectory. The deflection in the case of general nonlocal nonlinearity acts the same as that in the case of self-induced harmonic potential.

However, the evolution of the intensity pattern of the combined beam would be quite different for different degrees of nonlocality. The reason is as follows: In the case of strong nonlocality, the potential agrees well with the harmonic one. Therefore, the propagation characteristics of the two constituent beams and thereby the combined field would be the same as that predicted by the analytical solution [i.e., Eq. (24)]. But, with the decrease of the degree of nonlocality, the potential induced by the nonlinear refractive index gradually deviates from the harmonic one. Therefore, we can reasonably expect that the evolution of the combined beam would be more different from the prediction obtained based on Eq. (24).

In Fig. 4, we numerically simulate Eq. (49) to verify the above predictions. In numerical simulation, we assume that the material is with nonlocal Gaussian response [10,12,21], i.e.,

$$R(\mathbf{r}) = \frac{1}{2\pi w_m^2}\exp\left(-\frac{r^2}{2w_m^2}\right). \quad (51)$$

where w_m represents the characteristic length of the material response function. As shown in Fig. 4, when the degree of nonlocality is strong enough ($\sigma = w_m/w_0 \geqslant 10$), the numerical result is in good agreement with the analytical solution [i.e., Eq. (24)], which is obtained based on the assumption of self-induced harmonic potential. With the decrease of the degree of nonlocality, the numerical result deviates more from the analytical solution. When the degree of nonlocality is reduced to $\sigma = 5$ (row 3), although the shape of the intensity pattern of the numerical result still approximates well to the analytical result, the azimuthal orientation is slightly different from the analytical result (the deflecting beam rotates a little slower than theoretically predicted). However, when the degree of nonlocality is reduced to $\sigma = 1.5$ (row 4), not only the azimuthal orientation but also the pattern shape are

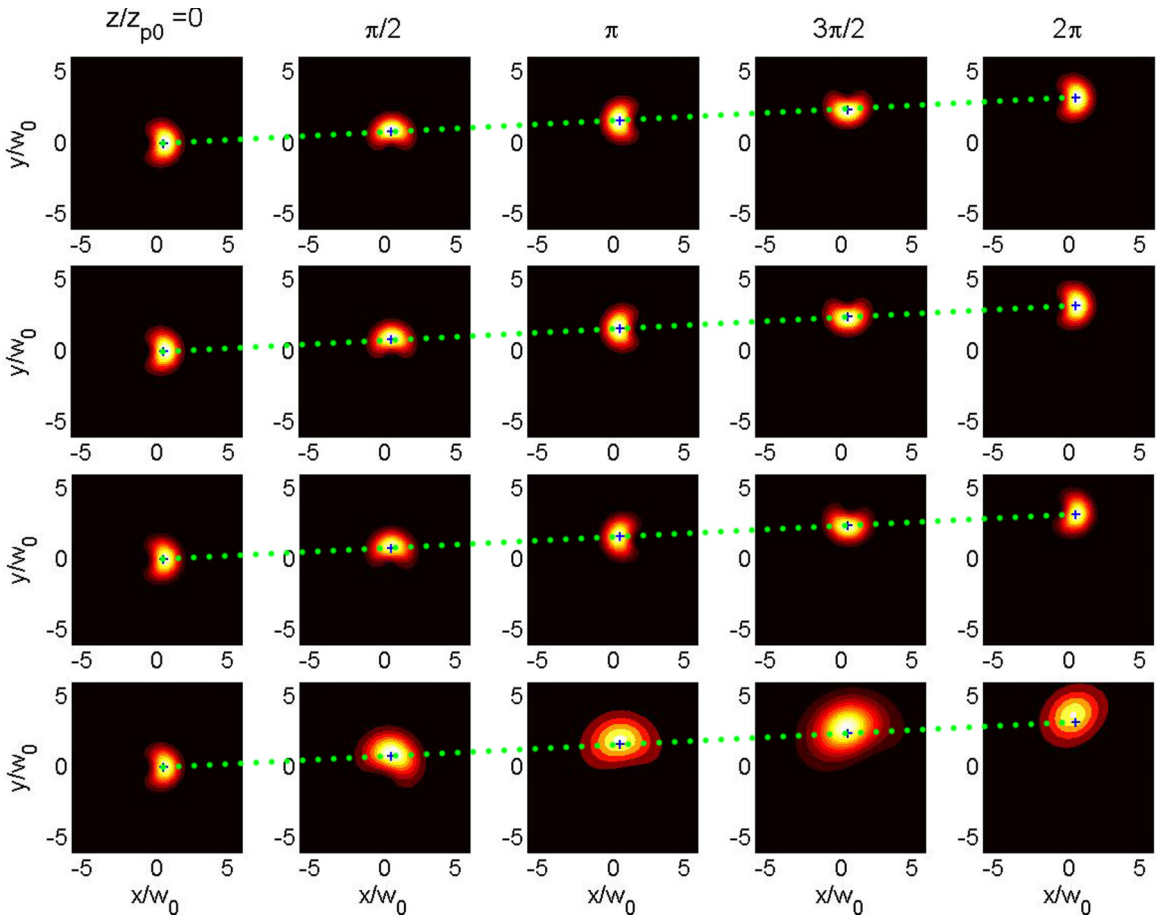

FIG. 4. The comparison of the propagation dynamics of the deflecting beam based on the analytical solution [Eq. (24), row 1] and that based on the numerical simulation of Eq. (49) for different degrees of nonlocality (rows 2–4). In rows 2–4, the degrees of nonlocality are $\sigma = w_m/w_0 = 10$, 5, and 1.5, respectively. $\delta = 0$, $b = 1$, and $P_0 = P_c$.

distinctly different from the analytical result. It is noted that the slope of the deflection is always identical to that obtained from the analytical solution [i.e., Eq. (24)], whatever the degree of nonlocality is, just as expected.

V. CONCLUSION

In conclusion, we have discovered another effect in self-induced harmonic potentials, i.e., magnitude- and orientation-steerable beam deflection. The input field for the deflecting beam is a combined field composed of a fundamental Gaussian beam and a (0,1) mode Laguerre-Gaussian beam. The magnitude and orientation of the deflection can be steered by tuning the ratio and the initial phase difference between the two input constituent beams, respectively. During propagation, the beam rotates around the deflecting straight trajectory that the mass center (not the constituent beams' center) undergoes. We have also extended the study to the general case of nonlocality and numerically simulated the general nonlocal nonlinear Schrödinger equation. It is shown that, in the case of strong nonlocality, the numerical result is in good agreement with the analytical solution based on the assumption of self-induced harmonic potential. With the decrease of the degree of nonlocality, the shape and azimuthal orientation of the combined beam become increasingly different from the analytical results. However, the slope of the deflection is always identical to the analytical result, whatever the degree of nonlocality is. The 2D-steerable beam deflection might be of interest for the applications in all-optical information processing.

ACKNOWLEDGMENT

This research was supported by the National Natural Science Foundation of China (Grants No. 11174090, No. 11174091, and No. 61575068).

[1] M. Newstein and K. Lin, Laguerre-Gaussian periodically focusing beams in a quadratic index medium, IEEE J. Quantum Electron. **23**, 481 (1987).

[2] Y. Q. Zhang, X. Liu, M. R. Belić, W. P. Zhong, M. S. Petrovic, and Y. P. Zhang, Automatic Fourier transform and self-Fourier beams due to parabolic potential, Ann. Phys. **363**, 305 (2015).

[3] J. Chen, F. S. Zhang, K. Bian, C. J. Jiang, W. Hu, and D. Q. Lu, Dynamics of shape-invariant rotating beams in linear media with harmonic potentials, Phys. Rev. A **99**, 033808 (2019).

[4] Y. Q. Zhang, X. Liu, M. R. Belić, W. P. Zhong, Y. P. Zhang, and M. Xiao, Propagation Dynamics of a Light Beam in a Fractional Schrödinger Equation, Phys. Rev. Lett. **115**, 180403 (2015).

[5] Y. Q. Zhang, X. Liu, M. R. Belić, W. P. Zhong, F. Wen, and Y. P. Zhang, Anharmonic propagation of two-dimensional beams carrying orbital angular momentum in a harmonic potential, Opt. Lett. **40**, 3786 (2015).

[6] Y. Q. Zhang, M. R. Belić, L. Zhang, W. P. Zhong, D. Y. Zhu, R. M. Wang, and Y. P. Zhang, Periodic inversion and phase transition of finite energy Airy beams in a medium with parabolic potential, Opt. Express **23**, 10467 (2015).

[7] M. A. Bandres and J. C. Gutiérrez-Vega, Airy-Gauss beams and their transformation by paraxial optical systems, Opt. Express **15**, 16719 (2007).

[8] A. W. Snyder and D. J. Mitchell, Accessible solitons, Science **276**, 1538 (1997).

[9] D. M. Deng and Q. Guo, Ince-Gaussian solitons in strongly nonlocal nonlinear media, Opt. Lett. **32**, 3206 (2007).

[10] S. Lopez-Aguayo and J. C. Gutiérrez-Vega, Elliptically modulated self-trapped singular beams in nonlocal nonlinear media: Ellipticons, Opt. Express **15**, 18326 (2007).

[11] W. P. Zhong and L. Yi, Two-dimensional Laguerre-Gaussian soliton family in strongly nonlocal nonlinear media, Phys. Rev. A **75**, 061801(R) (2007).

[12] D. Briedis, D. E. Petersen, D. Edmundson, W. Krolikowski, and O. Bang, Ring vortex solitons in nonlocal nonlinear media, Opt. Express **13**, 435 (2005).

[13] D. M. Deng, X. Zhao, Q. Guo, and S. Lan, Hermite-Gaussian breathers and solitons in strongly nonlocal nonlinear media, J. Opt. Soc. Am. B **24**, 2537 (2007).

[14] W. P. Zhong and M. R. Belić, Three-dimensional optical vortex and necklace solitons in highly nonlocal nonlinear media, Phys. Rev. A **79**, 023804 (2009).

[15] W. P. Zhong, L. Yi, R. H. Xie, M. R. Belić, and G. Chen, Robust three-dimensional spatial soliton clusters in strongly nonlocal media, J. Phys. B **41**, 025402 (2008).

[16] L. M. Song, Z. J. Yang, X. L. Li, and S. M. Zhang, Controllable Gaussian-shaped soliton clusters in strongly nonlocal media, Opt. Express **26**, 19182 (2018).

[17] Q. Guo, B. Luo, F. H. Yi, S. Chi, and Y. Q. Xie, Large phase shift of nonlocal optical spatial solitons, Phys. Rev. E **69**, 016602 (2004).

[18] D. Q. Lu, Q. Zhan, Q. L. Duan, and W. Hu, Power-variation-induced three-dimensional nonuniform scaling of beams in strongly nonlocal nonlinear media, Phys. Rev. A **87**, 023815 (2013).

[19] D. Q. Lu, W. Hu, Y. J. Zheng, Y. B. Liang, L. G. Cao, S. Lan, and Q. Guo, Self-induced fractional Fourier transform and revivable higher-order spatial solitons in strongly nonlocal nonlinear media, Phys. Rev. A **78**, 043815 (2008).

[20] S. G. Ouyang, W. Hu, and Q. Guo, Light steering in strongly nonlocal nonlinear medium, Phys. Rev. A **76**, 053832 (2007).

[21] A. I. Yakimenko, V. M. Lashkin, and O. O. Prikhodko, Dynamics of two-dimensional coherent structures in nonlocal nonlinear media, Phys. Rev. E **73**, 066605 (2006).